Paleoceanography and Paleoclimatology

RESEARCH ARTICLE
10.1029/2019PA003743

Key Points:
- We reconstructed the AAIW and PDW ventilation and geometry using δ13C, δ18O, and benthic foraminifera assemblages
- We observe a deepening of the AAIW during SO upwelling events during Termination I
- This deepening is probably accompanied by a southern extension of the AAIW

Supporting Information:
- Supporting Information S1
- Table S1
- Table S2

Correspondence to:
N. A. Haddam,
haddamn@gmail.com;
anhaddam@ifremer.fr

Citation:
Haddam, N. A., Michel, E., Siani, G., Licari, L., & Dewilde, F. (2020). Ventilation and expansion of intermediate and deep waters in the Southeast Pacific during the last termination. *Paleoceanography and Paleoclimatology*, *35*, e2019PA003743. https://doi.org/10.1029/2019PA003743

Received 1 AUG 2019
Accepted 11 MAY 2020
Accepted article online 12 JUN 2020

Ventilation and Expansion of Intermediate and Deep Waters in the Southeast Pacific During the Last Termination

N. A. Haddam[1,2], E. Michel[2], G. Siani[1], L. Licari[3], and F. Dewilde[2]

[1]GEOPS Géosciences Paris-Sud, CNRS, Université de Paris Sud Paris Saclay, Orsay Cedex, France, [2]LSCE/IPSL Laboratoire des Sciences du Climat et de l'Environnement, CEA-CNRS-UVSQ, Orme des Merisiers, Saint-Aubin, France, [3]Centre Européen de Recherche de d'Enseignement des Géosciences de l'Environnement, CNRS, Université d'Aix-Marseille, Aix-en-Provence Cedex, France

Abstract We investigate the geometry and ventilation of the water masses within bathyal depths (~1,500 to ~2,500 m) of the Southeast Pacific (SEP), inferring the lower depth limit variations of the Antarctic Intermediate Water (AAIW) since ~22 kyr cal. BP. We use three cores collected at the upper limit of the Pacific deep waters, between 41°S and 49°S, and one core at a greater depth within this same water mass, at 46°S. The benthic foraminiferal assemblages and carbon and oxygen isotopes are used to show strong linkages between the timing of the deglacial Southern Ocean upwelling events and changes in the vertical extension and ventilation of the AAIW. In accordance with local/sublocal oxygen reconstructions, we propose at least three states of ventilation-AAIW vertical extension: (i) the late glacial and the Antarctic Cold Reversal (ACR): AAIW depth-limit shoals, as its formation zone moves northward; (ii) the deglaciation (excluding the ACR): the [O_2] enrichment of the AAIW and the dominance of benthic species *Trifarina angulosa* indicate ventilated AAIW, along with a deepening of its lower limit; and (iii) the Holocene: enhanced influence of the Pacific deep water at bathyal depths (1,500–2,500 m) in the SEP north of ~46°S and the circumpolar deep water south of ~46°S.

1. Introduction

Past hydrological variations in the Southeast Pacific (SEP) are of wide interest, as this region is considered critical for Antarctic Intermediate Water (AAIW) formation (McCartney, 1977). This water mass is an important component of the Meridional Overturning Circulation (MOC), therefore playing a major role in the transfer of heat, fresh water, nutrients, and carbon from the high to low latitudes of the Southern Hemisphere (Fischer et al., 2010; Talley, 1999).

Several oceanographic studies focused on the AAIW have shown that most of this water mass originates from the high latitudes of the SEP, south of the Polar Front (PF; e.g., McCartney, 1977), or between the PF and the Subantarctic Front (SAF; Hartin et al., 2011). The AAIW originates from the upwelling of the CDW or UCDW at these high latitudes and is then transported northward around ~500 to ~1,500 m depths (Sloyan et al., 2010). It then flows northward, before turning westward in the lowermost latitudes of the Pacific Ocean, following the subtropical gyre before reaching the Southwestern (SW) Pacific, north of New Zealand (Tomczak & Godfrey, 1994). Past variations of the SW part of the AAIW has been thoroughly studied using several physical and geochemical tracers (e.g., Bostock et al., 2004, 2010; Bostock, Sutton, et al., 2013; Durand et al., 2018; Elmore et al., 2015; Hines et al., 2015; Pahnke & Zahn, 2005; Tapia et al., 2015). Previous studies, focusing on the Southwest Pacific Ocean, suggest a decrease in intermediate and deep water ventilation during cold periods (e.g., the Antarctic Cold Reversal, ACR, or the Last Glacial Maximum, LGM) (Bostock, Barrows, et al., 2013; Hines et al., 2015) while others suggest that during the interglacial stages of the last 400 kyr cal. BP, the AAIW was warmer and well ventilated (Elmore et al., 2015). Furthermore, their findings proposed a shoaling of the lower limit of the AAIW during glacial stages (Elmore et al., 2015), with the extended Antarctica winter sea ice related to a shallower AAIW subduction in the SW Pacific, whereas warmer conditions lead to a latitudinal expansion of the AAIW (Ronge et al., 2015).

Fewer studies address the intermediate depths water masses in southeastern Pacific ocean compared to the SW sector. To date, some of them suggest an increase in AAIW production and/or deepening of the lower

boundaries of this water mass in the SEP during glacial periods (Martínez-Méndez et al., 2013; Muratli et al., 2010).

Despite these diverse contributions, some critical issues need to be clarified, that is, the formation mechanisms of the AAIW, as well as its relationship with the Southern Ocean (SO) upwellings. For example, it is unclear whether and how the geometry and ventilation of the intermediate water masses could be influenced by the SO upwelling variation, which occurred throughout the deglaciation (Anderson et al., 2009; Siani et al., 2013).

The aim of this study is to investigate the ventilation changes and the geometrical variations at intermediate depth (~1,500 to ~2,500 m) in the SEP since the late glacial (~22 kyr). To accomplish this, we selected four cores collected along the south Chilean margin and located within the upper boundary of the Pacific deep water (PDW) and at the transition between the PDW and the circumpolar deep water (CDW), respectively, following a latitudinal transect between 41°S to 49°S. We then reconstruct the water column geometry variation between ~1,500 and ~2,500 m since the late glacial and show the relationship of the enhanced upwelling events at the Antarctic divergence and the production of AAIW during the deglaciation, through a coupled approach, using the oxygen and carbon isotopic records ($\delta^{18}O$ and $\delta^{13}C$) on benthic foraminifera and faunal assemblages.

2. Study Area

2.1. Atmospheric and Continental Setting

The studied area is located in the SEP (Figure 1) under the influence of the southern westerly winds (SWWs), which are intercepted by the southern South America landmass and producing considerable amount of precipitation. According to the NCEP/NCAR reanalysis data (Kalnay et al., 1996), the SWWs extend from ~49°S to ~53°S during austral summer. In winter, the SWWs display weaker velocities and a broader latitudinal extent. On the continent, the precipitation rates display a north-south increasing gradient (mean annual precipitations of ~2,000 to ~3,000 mm $year^{-1}$, at, respectively, ~42°S to ~50°S; Garreaud et al., 2013) and are intercepted by two parallel approximately north-south mountain chains, the coastal range (less than ~500 m above sea level) and the Andean Cordillera (less than ~3,000 m above sea level). The result of strong precipitation produces a high sedimentary transport to the Chilean margin.

2.2. Surface Hydrography

One of the major hydrological features of the SEP (East of ~110°W) is the Antarctic circumpolar current (ACC). It extends from the Southern ACC front (SACC and/or Southernmost boundary of the ACC) in the south to the subtropical front (STF) in the north (Orsi et al., 1995; Rintoul et al., 2001; Stramma et al., 1995), which marks the northernmost reach of Subantarctic zone (Peterson & Stramma, 1991). Between the SACC and the STF, the SAF and PF are the principal fronts of the ACC (with larger ACC speed associated with these fronts). In the SEP, the mean northern boundary of the ACC is defined at ~50°S (Park et al., 2019) with both the SAF and the PF forced into the Drake Passage. Our studied area is located between the STF in the north, which is not well defined near the South American Coast, and the SAF and PF (respectively positioned at ~56°S and ~58°S in the Drake Passage) in the south (Figure 1b). A northern branch of the ACC divides in two coastal currents: the northward flowing Peru-Chile current (PCC) and the southward flowing Cape-Horn current (CHC) (Figure 1b) (Silva et al., 2009).

Satellite data indicate that the SEP is characterized by relatively high concentration of chlorophyll throughout the year (~3 to ~10 mg/m^3 near the coast between 40°S and 47°S) (Figure 1c; Ocean Biology Processing Group, 2014). There is however a seasonal variation in the production of photosynthesizing organisms. The maximum of the production occurs during the austral spring, whereas the minimum during the austral autumn (e.g., Pinochet et al., 2019).

2.3. Deep Sea Circulation

Several water masses underlie the surface waters in the SEP along the Chilean margin. The northward flowing low-salinity AAIW lies between 600 and 1,300 m depth (Figure 1a; Bostock et al., 2010; Silva et al., 2009; Talley, 2013). The SEP is the principal region of formation for this water mass (e.g., McCartney, 1977). Studies using Argo data have also showed that there are several other regions of AAIW formation along

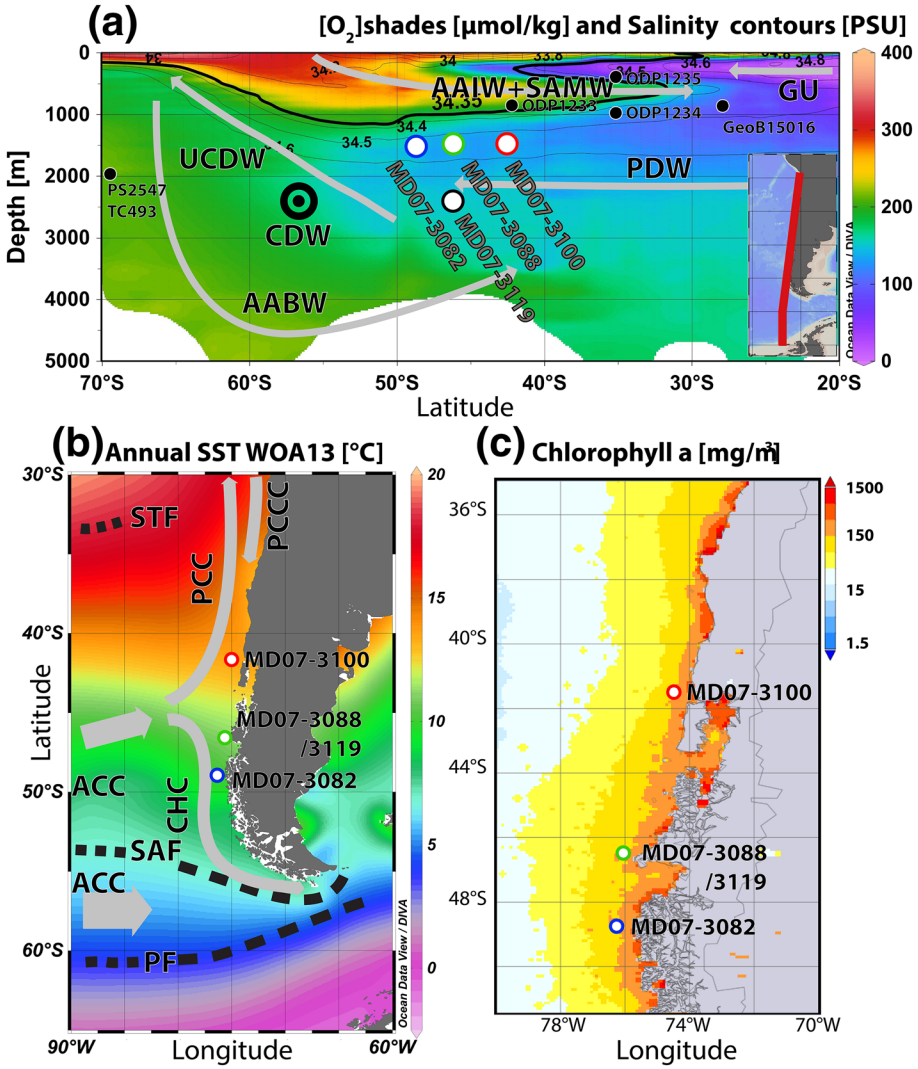

Figure 1. (a) Depth transect in the SEP showing the salinity, the [O_2] (World Ocean Atlas 2013; WOA, Boyer et al., 2013), and the principal water masses: Antarctic bottom water, AABW; Antarctic intermediate water, AAIW; Gunther undercurrent, GU; Pacific deep waters, PDW; Subantarctic mode water, SAMW; (upper) circumpolar deep water (U)CDW. In addition to the cores studied here (colored dots), the black dots indicate the position of the ODP Sites 1233, 1234, and 1235 (Muratli et al., 2010); the position of core GeoB15016 (Martínez-Méndez et al., 2013); and the position of core site PS2547/TC493 (Lu et al., 2016). (b) Annual Sea surface temperatures (SST) according to World Ocean Atlas 2013 (WOA, Boyer et al., 2013), and the principal surface currents and oceanic fronts in the SEP: Antarctic circumpolar current, ACC; Cape Horn current, CHC; Peru-Chile current, PCC; Peru-Chile counter current, PCCC; polar front, PF; Subantarctic front, SAF; subtropical front, STF. (c) Annual chlorophyll a concentration (Ocean Biology Processing Group, OBPG, 2014). The figure was made using ocean data view (Schlitzer, 2020).

the SAF (Hasson et al., 2012; Herraiz-Borreguero & Rintoul, 2011; Qu et al., 2008; Sallée et al., 2010). The AAIW subduction from the surface to intermediate depths is probably driven by several processes such as air-sea fluxes, Ekman transport, eddy and turbulent mixing, and mixing at the base of the mixed layer (McCartney, 1982; Ribbe & Tomczak, 1997; Rintoul & England, 2002; Sloyan & Rintoul, 2001). However, the exact processes of its formation are still unclear (for a detailed review, see Bostock, Sutton, et al., 2013, and the references cited therein). The present-day AAIW is characterized, in the SEP (87°W), by $\delta^{13}C$ and salinity values ranging from 0.6‰ to 1.7‰ and from 34.2 to 34.35 PSU, respectively (Bostock et al., 2010; Bostock, Barrows, et al., 2013, and the references therein).

Below the AAIW, the nutrient-rich/oxygen-poor (less than ~180 µmol/kg) PDW flows southward, from 1,300 to 3,000 m (Figure 1a) (e.g., Leth et al., 2004; Talley, 2008, 2013). Low oxygen values also

characterize the southward flowing Gunther Undercurrent (equatorial subsurface water), which is associated with the oxygen minimum zone (OMZ) of the SE Pacific Ocean (e.g., Leth et al., 2004). This current brings oxygen-depleted, nutrient-rich waters to the south at >40°S at ~300 m depth, before being compensated by the oxygen-rich AAIW (Figure 1a). Further south (~50°S), the AAIW is underlain by the CDW (Figure 1a) where the upper layers of this water mass (hereafter UCDW) fills the intermediate depths (Talley, 2013). The CDW is controlled by the ACC (e.g., Tomczak & Godfrey, 2001), and its upper component the UCDW upwells south of the PF, flowing then northward and forming AAIW (Figure 1a) (Tsuchiya & Talley, 1998). The CDW includes deep waters from the different oceanic basins (Talley, 2013) and is characterized by relatively higher [O_2] compared to the PDW (greater than ~180 μmol/kg) (Talley, 2013; Figure 1a). In our studied area, the AAIW shows highest [O_2] at 600 m (from ~230 to greater than ~270 μmol/kg, between ~40°S and ~50°S) while in the upper limit of the PDW (1,400 m) the [O_2] presents values from ~128 to ~150 μmol/kg (Silva et al., 2009).

3. Material and Methods

Four CALYPSO cores were retrieved from the SEP following a latitudinal transect, off the coast of Chile: MD07–3100 (41°36′S, 74°57′W, 1,609 m depth, and 29.83 m long), MD07–3119 (46°05′S, 76°06′W, 2,523 m, and 32.54 m long), MD07–3088 (46°04′S, 75°41′W, 1,536 m, and 18.91 m long), and MD07–3082 (49°10′S, 76°34′W, 1,792 m, and 20.46 m long) (Figures 1a and 1b). These cores were collected in 2007 during the PACHIDERME cruise on the R/V Marion Dufresne (Kissel, 2007). In the studied cores, the sediments are dominated by olive-brown to light-olive silty clays, and by the presence of several tephra layers.

3.1. Age Models

The age models of cores MD07–3088, MD07–3100, and MD07–3082 were previously described in Haddam et al. (2018). For core MD07–3119, 15 ^{14}C ages were measured on the planktonic foraminifera *Globigerina bulloides* (Table S1 in the supporting information) and converted to calendar ages using the same reservoir ^{14}C age correction as for the nearby core MD07–3088 (Haddam et al., 2018; Siani et al., 2013) and SHCal13 (Hogg et al., 2013) based on oxcal software (Bronk Ramsey & Lee, 2013).

3.2. Foraminifera Stable Isotope Measurements (δ^{18}O and δ^{13}C)

Stable oxygen and carbon isotopes were measured on planktonic and benthic foraminifera. Concerning the planktonic foraminifera, the species *Globigerina bulloides* (d'Orbigny, 1826) (250–315 μm fraction, ~4 to ~30 shells for each sample) was used for δ^{18}O and δ^{13}C analyses, every 10 cm for MD07–3100 and MD07–3119, and every 5 cm for MD07–3088 and MD07–3082 (total samples of 285, 321, 245, and 196, respectively, and including the replicates). The epibenthic foraminifera species *Cibicidoides wuellerstorfi* (Schwager, 1866), *Cibicidoides pachyderma* (Rzehak, 1886), *Cibicidoides kullenbergi* (Parker, 1953), *Heterolepa bradyi* (formerly *Cibicides bradyi*; Trauth, 1918) (Figure S1) and endobenthic foraminifera species *Globobulimina affinis* (d'Orbigny, 1839) and *G. pyrula* (d'Orbigny, 1846) were picked from the sediments of core MD07–3100; *C. wuellerstorfi*, *G. affinis*, and *G. pyrula* in core MD07–3088 and MD07–3119; *C. wuellerstorfi* in core MD07–3082 (425, 254, 72, and 180 samples, respectively). Ideally, one species would have been used for each microhabitat (e.g., *C. wuellerstorfi* for the epifauna and *G. affinis* for the infauna), but their availability was not continuous downcore. However, we used a correction factor for δ^{13}C values for *C. pachyderma*, *H. brady*, and *C. kullenbergi* (+0.3‰, +0.89‰, and +0.64‰, respectively). This correction factor represents the mean offset between the δ^{13}C values of these three species and those measured on *C. wuellerstorfi* according to the levels where two or more of these species were available and measured. We used the same approach for *G. affinis* and *G. pyrula* (Table S2).

Each sample was cleaned using methanol and ultrasounds and then was oven-grilled at 380°C during 45 min prior to the isotopic analysis. Isotopic analyses were performed at Laboratoire des Sciences du Climat et de l'Environnement on an Optima VG, a Finnigan Delta +, and a GV Isoprime mass spectrometers. The measurements are reported versus Vienna Pee Dee Belemnite standard (VPDB) defined with respect to NSB19 standard. The mean external reproducibilities (1σ) of carbonate standards measured on the Optima VG are ±0.06‰ and ±0.04‰ for δ^{18}O and δ^{13}C, respectively. For the other two mass spectrometers, the reproducibilities are, respectively, ±0.05‰ and ±0.03‰ for δ^{18}O and δ^{13}C. For NBS-18, the δ^{18}O and δ^{13}C values

obtained are −23.27 ± 0.10‰ and −5.01 ± 0.3‰ VPDB, respectively. Reproducibility of the measurements on each species group of each core is presented in Table S2.

3.3. Benthic Foraminifera Faunal Assemblages

We used the meio-faunal observations (benthic foraminifera) to qualitatively assess and compare the bottom water ventilation variations between all the considered cores and time intervals. Samples were wet sieved, and the benthic foraminifera were counted in the >150 μm fraction. The resolution of the benthic assemblages analyzes was adapted according to the faunal variability. We thus counted 58 samples for core MD07–3100 (among which nine samples had less than 250 individuals counted in the first 90 cm of the core; Figure S2). For core MD07–3082, we counted 12 samples due to the low assemblage variability (qualitatively assessed) in this core (among which five samples had less than 250 individuals counted in the last 120 cm of the core; Figure S3). The counted benthic foraminifera were picked and stored in Chapman slides. The benthic foraminifera taxonomic identification reaches species level whenever possible, based on the descriptions of Loeblich and Tappan (1987).

4. Results

4.1. Benthic Foraminifera Carbon and Oxygen Stable Isotopes

4.1.1. Carbon Isotopes

Carbon isotopes measurements performed on the epibenthic foraminifera genera *Cibicides* and *Cibicidoides* (grouped as *Cibicides spp*.) are displayed in Figure 2a for the four cores. During the late glacial (22–18 kyr) and the first part of the deglaciation, the three shallower cores bathed today by the PDW (above 1,792 m) indicate a similar behavior despite some slight differences related to different sedimentation rates and sampling resolution. The lower $\delta^{13}C$ values characterize the late glacial, approximately −0.1‰, followed by a rapid increase between ~17 to ~15.5 kyr, reaching ~0.35‰. The increasing $\delta^{13}C$ trend is interrupted by a $\delta^{13}C$ lowering centered at ~14 to 12.5 kyr and followed by a regular incremental increase since about 11 kyr, more marked for core MD07–3082. The deepest MD07–3119 core indicates lower mean $\delta^{13}C$ values of approximately −0.4‰ during late glacial, followed after 17 kyr by an increasing trend. From 9.5 kyr the MD07–3119 $\delta^{13}C$ record indicates similar values than the shallow MD07–3088 and MD07–3100 cores, suggesting that these sites are bathed by the same water mass.

4.1.2. Oxygen Isotopes

The $\delta^{18}O$ analyses measured on the benthic foraminifera of the four considered cores are displayed in Figure 2 for the last 22 kyr.

The highest $\delta^{18}O$ values are observed within the late glacial and range from ~4.1‰ for core MD07–3088 to ~4.5‰ for cores MD07–3100 and MD07–3119. Then, from ~17 to ~11 kyr, the $\delta^{18}O$ records of the shallower cores indicate a two-step rapid decrease, interrupted by steady to slightly higher values from ~14 to ~12.5 kyr. A slow $\delta^{18}O$ decrease marks the entrance to the Holocene until ~7 kyr where steady values at ~2.6‰ are attained for the three cores. It is interesting to note that the MD07–3082 $\delta^{18}O$ decreasing trend from ~14 to ~7 kyr presents values slightly higher than those from MD07–3088 and MD07–3100 ones. For MD07–3119 core, the $\delta^{18}O$ values indicate a rapid decrease starting at ~14.3 kyr, interrupted from ~12.8 to ~11.8 kyr with values reaching ~3.7‰. No $\delta^{18}O$ data are available between ~11.6 and ~9.3 kyr due to the lack of *C. wuellerstorfi* in the sediment during this interval. After ~9 kyr, a slight $\delta^{18}O$ decrease, from 3‰ to 2.6‰, characterizes the whole Holocene period.

4.2. Bottom Water Oxygen Qualitative Reconstruction

To assess the qualitative evolution of the bottom water oxygen concentration during the last 22 kyr, reconstructed $[O_2]$ of the bottom water of cores MD07–3100, 3,088 and 3,119 is represented in Figure 2c. The $[O_2]$ was calculated from the $\Delta\delta^{13}C$ between *Cibicides* spp and *Globobulimina* spp following the calibration of Hoogakker et al. (2015). This method allows the reconstruction of bottom water $[O_2]$ with values lying between 55 and 235 μmol/kg (~1.3 and ~5.4 mmol/l) (Hoogakker et al., 2015). Despite the relatively large error for bottom $[O_2]$ reconstruction (reproducibilities of the $\delta^{13}C$ measurements when propagated in the calibration equation show largest error for core MD07–3088, ± ~30 μmol/kg; Table S2), significant changes are observed in the three core records (Figure 2c).

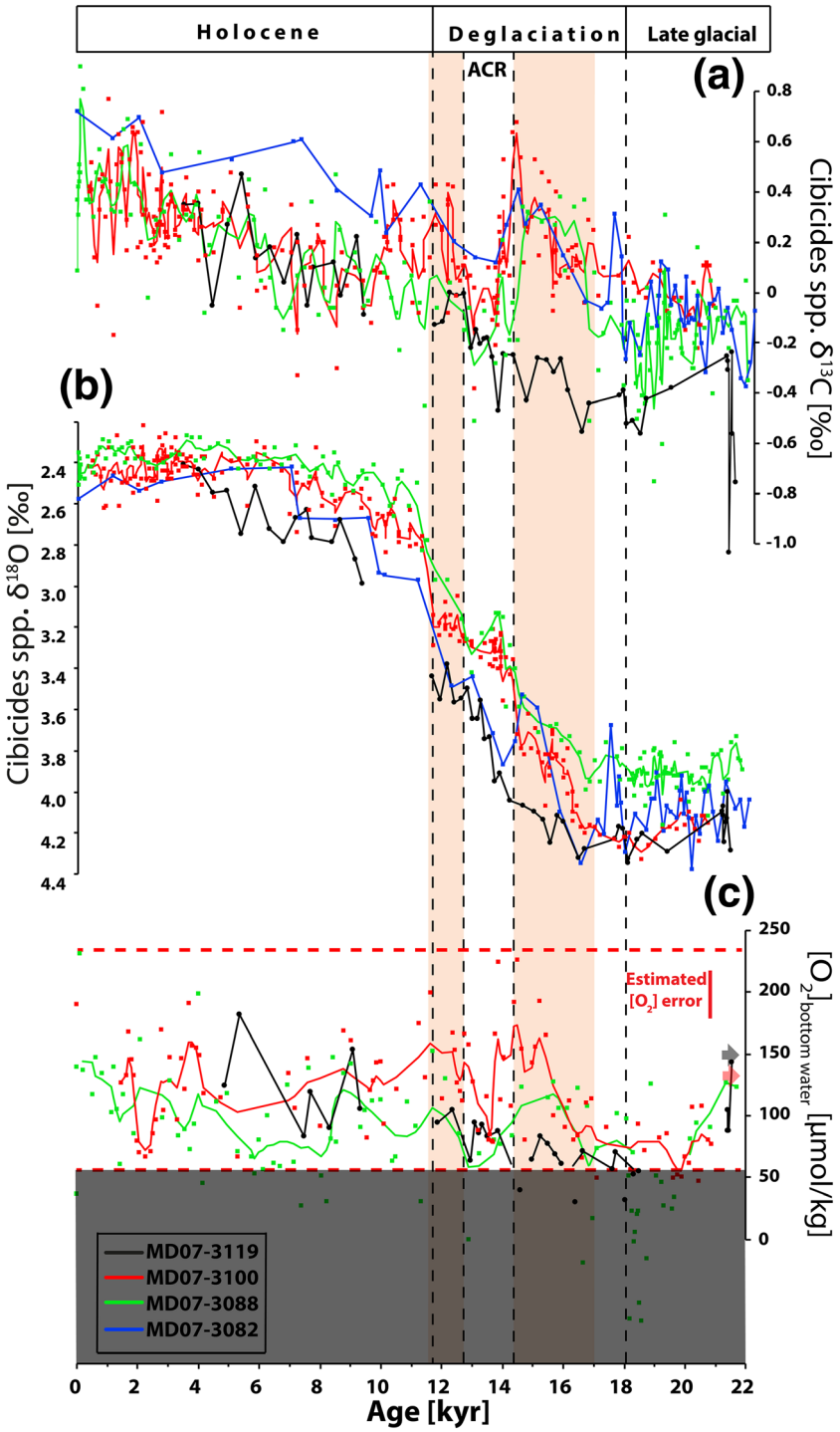

Figure 2. (a) *Cibicides* spp. δ^{13C} and (b) *Cibicides* spp. $\delta^{18}O$ measured on the three considered cores. (c) $[O_2]$ reconstructed in cores MD07–3100, MD07–3119, and MD07–3088 following the calibration of Hoogakker et al. (2015). The horizontal red dashed lines represent the sensitivity limits of this calibration; the lower limit of the calibration is shaded. The vertical red line represents the estimated error for the estimations (± ~30 µmol/kg). The red arrow represents the actual $[O_2]$ value at 1,500 m according to Silva et al. (2009), and the black arrow at 2500 according to World Ocean atlas 2013 (WOA, Boyer et al., 2013). We used 3-point moving average to smooth MD07–3100 and MD07–3088 curves. Pink shading indicates the periods of Southern Ocean upwelling increase (Siani et al., 2013).

From 20 to 16.5 kyr [O_2] values are quite low, between ~55 and 75 μmol/kg or under the lower calibration limit (~55 μmol/kg). During the deglaciation, the shallower cores, MD07–3100 and MD07–3088 indicate two periods of sharp [O_2] increase, from ~16.5 to ~13.8 kyr and from ~12.8 to ~11.2 kyr, with values higher than 150 μmol/kg (~200 μmol/kg for MD07–3100). For the deepest core MD07–3119, the [O_2] values stay low until ~14.3 kyr and then increase up to ~11.8 kyr to reach ~100 μmol/kg. It is also important to consider that the Holocene is weakly represented for the deepest core, due to the scarcity of *Cibicides* individuals during that period. Overall, the few Holocene [O_2] values obtained for the three cores indicate concentrations reaching ~130 μmol/kg around 9 kyr and ~140 μmol/kg for the last 2 kyr, similar to the modern values (from ~110 to ~150 μmol/kg; Silva et al., 2009; WOA, Boyer et al., 2013; Figure 2c).

In details, for the shallower cores, large [O_2] variations occur during the Holocene, with lower [O_2] values around 10.5, 8, and 6 kyr, respectively. Then, [O_2] values increase from ~50 μmol/kg to reach ~140 μmol/kg in the last millennia for core MD07–3088, similar to the modern observed value. For core MD07–3100, [O_2] values increase rapidly to reach ~170 μmol/kg at ~4 kyr, and the water remains oxygenated until the Late Holocene except for a short event from 3 to 2 kyr, when [O_2] concentrations drop to 70 μmol/kg. In summary, the reconstructed [O_2] is higher for core MD07–3100 at 41°S than for core MD07–3088 at 46°S (Figure 2c).

4.3. Benthic Foraminifera Abundances

Due to the lack of *Globobulimina* spp in core MD07–3082, we were not able to reconstruct the bottom [O_2] at 49°S. In order to have a qualitative insight on our core's bottom water ventilation variations, we thus investigated the faunal content of MD07–3082 and MD07–3100 cores.

We counted from 100 to 500 benthic foraminifera individuals in core MD07–3100 and ~100 to 450 in core MD07–3082, respectively. We chose to show the most abundant (with a continuous downcore presence and/or showing greater than ~10% relative abundances) and ecologically significant species, grouped by genera, in Figure 3. Over the last 22 kyr, the benthic foraminifera assemblage in core MD07–3100 is generally dominated by *Uvigerina peregrina* (which is the species largely dominating this group (greater than ~80% of *U. spp*.) followed by *U. auberiana* (d'Orbigny, 1839), *U. c.F. gracilis* (Reuss, 1851), *U. phlegeri* (Le Calvez, 1958), and *U. proboscidea* (Schwager, 1866) (Table S3; Figure 3a), except from 17 to 16 kyr, where it is replaced by *Nonionella auris* (d'Orbigny, 1839), *Bulimina* spp (largely dominated by *B. striata* "*d'Orbigny in* Guérin-Méneville, 1832," and including rare occurrences of *B. alazanensis* "Cushman, 1927"; *B. marginata* "d'Orbigny, 1826"; *B. c.F. gibba* "Fornasini, 1902"), *Cibicidoides* spp and *Trifarina angulosa* (Williamson, 1858), and from 15 to 13.5 kyr, 12.7 to 12.2 kyr, and 11 to 10.8 kyr where *T. angulosa* and/or *Bulimina* spp dominates the assemblage. The relative percentage of *Uvigerina* spp varies from <5% (~16.8 kyr) to ~60% (~19.7 kyr). The lowest values are found from ~12 to ~18 kyr. The occurrence of *T. angulosa* is concentrated between ~17 and ~9.5 kyr with a maximal abundance at ~13.7 kyr where it represents ~35% of the total assemblage. This species percentages are >5% only between ~10 and ~16.8 kyr. The species from the genera *Cibicidoides* do not exceed 25% with low percentages (<10%) found mainly between ~14.5 and ~10 kyr.

The benthic foraminifera assemblage of core MD07–3082 (Figure 3b) is dominated by the species of the *Cibicidoides* group in the interval younger than ~16 kyr reaching 40% of the total assemblage at ~14 kyr. By contrast, *Uvigerina* spp represents the dominant taxon, reaching a maximum value of 35% of the total assemblage between 20 to 16 kyr.

5. Discussion

Today, the four studied cores are bathed by the PDW of which the two shallower (MD07–3100 and MD07–3088) sit at the lower boundary of AAIW. By contrast, the southernmost one (MD07–3082) is the closest to the CDW (Figure 1). The comparison between the different proxy records, that is, $\delta^{18}O$, $\delta^{13}C$, [O_2] values, and faunal assemblages (when the [O_2] reconstructions are not available) (Figure 2a), might provide information about the past evolution of these water masses since the late glacial (~22 kyr).

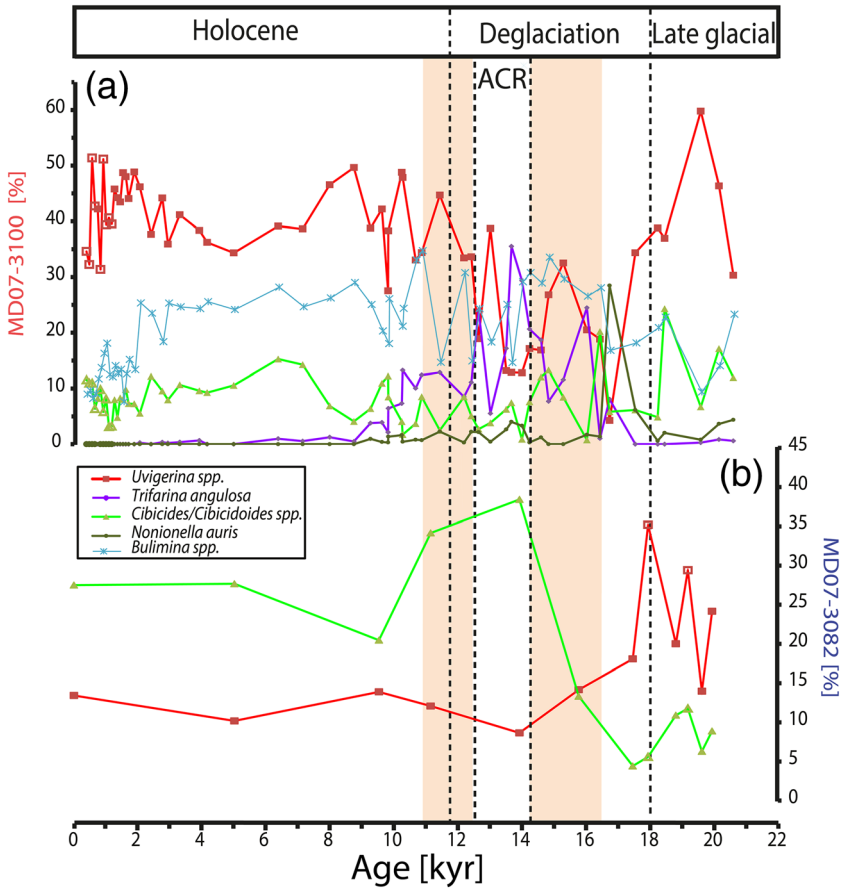

Figure 3. Most abundant benthic foraminifera species in core MD07–3100 (a) and MD07–3082 (b). Pink shading indicates the periods of Southern Ocean upwelling increase. Samples with less than ~250 foraminifera are represented by empty dots.

5.1. Late Glacial

Looking at the benthic $\delta^{18}O$ records in Figure 2b, a decrease of ~1.6‰ characterizes the interval from the late glacial to the late Holocene (<2 kyr). This $\delta^{18}O$ difference is larger than the mean oceanic change by ~0.5‰, indicating a glacial ocean that would be colder by ~2°C in agreement with previous results from the deep Pacific Ocean (Duplessy et al., 2002; Elderfield et al., 2010; Labeyrie et al., 2005; Waelbroeck et al., 2002). During the late glacial, the MD07–3082, MD07–3100, and MD07–3119 $\delta^{18}O$ records indicate similar values despite their different water depth, while core MD07–3088 displays lower $\delta^{18}O$ values (Figure 2b). The effect of the bottom water temperature difference, between the shallow and the deep cores, on the benthic foraminifera $\delta^{18}O$ could be compensated by the water oxygen isotopic composition. At the depth of MD07–3088, the water mass should be originating from higher latitude surface water, with lower isotopic composition. However, this does not explain how a significant difference of 0.2‰ is observed during the late glacial between core MD07–3088 and the other shallow cores (MD07–3100 and MD07–3082). This difference could be explained by enhanced vertical mixing at 46°S related to the presence of the Chilean Rise, modifying the seafloor architecture, and generating a major obstacle for the current dynamic (flowing on a north-south axis) at that location (Figure S4).

During the late glacial, the average $\delta^{13}C$ values for the three shallow cores (approximately −0.1‰) show a ~0.4‰ difference with MD07–3119 $\delta^{13}C$ values, indicating that the latter site is bathed by less ventilated water masses. Such a $\delta^{13}C$ depth gradient has been observed in different ocean basins, including the Pacific, during the LGM (Boyle & Keigwin, 1987; Curry et al., 1988; Curry & Oppo, 2005; Duplessy et al., 1988; Hodell et al., 2003; Michel et al., 1995), corresponding to two glacial separated overturning cells (Keeling &

Stephens, 2001; Michel et al., 1995; Toggweiler, 1999; Toggweiler et al., 2006). Thus, the $\delta^{13}C$ gradient indicates that the shallower cores were within the upper overturning cell while MD07–3119 lay within the deep overturning cell during the glacial period. These two separated cells might be related to the northward shift of the SWW (Toggweiler, 1999; Toggweiler et al., 2006) and/or to the latitudinal expansion of sea ice in the SO (Ferrari et al., 2014; Keeling & Stephens, 2001).

The reconstructed $[O_2]$ of cores MD07–3100, MD07–3088, and MD07–3119 for the late glacial is similar and among the lowest of the last 20 kyrs (Figure 2c). To extend the comparison of the ventilation variations up to 49°S, we compare the benthic foraminifera faunas between MD07–3100 (41°S) and MD07–3082 (49°S) cores. The foraminifera assemblages at 41°S and 49°S show both the dominance of *Uvigerina* spp and *Cibicidoides* spp. The largest percentage of *Uvigerina* spp (mostly *U. peregrina*) is observed during the late glacial for core MD07–3082 (Figure 3). We measured, using X-ray florescence, the Ba/Ti on the sediment of core MD07–3082 (Figure S5). From this ratio we observe higher Barium content during the Holocene, indicating increased organic matter supply (Croudace & Rothwell, 2015). This is in accordance with the enhanced Holocene phytoplankton production observed at 46°S in the sediment of core MD07–3088 (Duchamp-Alphonse et al., 2018). This enhanced food availability during the Holocene is not in accordance with the glacial dominance of *Uvigerina spp*, suggesting that the occurrence of this genus is more likely linked to a lower late glacial oxygenation. However, we cannot totally rule out any influence on the food supply on our assemblages (e.g., Hermelin & Shimmield, 1990; Jannink et al., 1998).

Only a few studies have focused on the past AAIW oxygen concentration in the SEP, showing a glacial increase of the AAIW oxygenation, inferred from redox-sensitive trace metal concentrations between 35°S and 41°S and ~500 and ~1,000 m (Muratli et al., 2010). The higher LGM AAIW $[O_2]$ was interpreted as a northward displacement of the AAIW source region (i.e., closer to their studied sites; 36°S to 41°S), probably associated with an increase in the AAIW production rate (Muratli et al., 2010). Jaccard and Galbraith (2011) compiled different studies devoted to the $[O_2]$ difference between the early Holocene and the LGM at different water depths. Their findings show that the $[O_2]$ LGM increase is coherent in most of the AAIW records of the eastern side of the Pacific Ocean. Interestingly, it has been proposed that the cold periods in the eastern Pacific (core GeoB-15,016 at 27.5°S) are characterized by a northern migration of the AAIW convection center possibly associated with a production increase and/or a deepening of its lower limit (Martínez-Méndez et al., 2013). Those studies are based on cores located farther north along the Chilean cost and at shallower depth (≤1,000 m). The reduced glacial oxygen concentration (compared to the Late Holocene) and the lower $\delta^{13}C$ values observed at ~1,600 m depth (approximately −0.1 compared to ~0.35 in average for core GeoB15016, 956 m) for cores MD07–3082, MD07–3088, and MD07–3100 indicate that the AAIW limit did not deepen down to these cores' locations and that they lie on the southern return path of the upper overturning cell. The relatively decreased early deglacial ventilation at ~70°S in the SO (core site PS2547/TC493; Lu et al., 2016), in agreement with the benthic faunal content of MD07–3082, confirms the influence of an oxygen poor CDW and/or PDW at ~49°S. The lower late glacial $[O_2]$ observed at 2,500 m depth for core MD07–3119 is also in agreement with the compilation of equatorial Pacific records, deeper than 2,000 m depth, that indicates lower oxygenation during the LGM than during the early Holocene (Jaccard & Galbraith, 2011).

5.2. The Last Deglaciation

The deglaciation in the SEP is affected by enhanced upwelling events at the Antarctic divergence (Anderson et al., 2009; Siani et al., 2013), as indicated by increase surface ^{14}C reservoir age and decreasing $\Delta^{14}C_{b\text{-}p}$ and $\Delta^{13}C_{b\text{-}p}$ from core MD07–3088 (Siani et al., 2013; Figure S6). During these upwelling events, the deep, old, nutrient-rich water masses are brought at the surface in the Antarctic divergence and are transferred via Ekman transport to the middle-high latitudes, affecting Antarctic and sub-Antarctic surface waters as well as newly formed SAMW and AAIW. The most prominent event occurs between ~16.5 and ~14.2 kyr, Event 1, whereas the second one between ~12.5 and ~10.8 kyr, Event 2. During Event 1, the $\delta^{18}O$ values of cores MD07–3100, MD07–3088, and MD07–3082 decrease rapidly and become similar at ~3.9‰ (Figure 2b). The $\delta^{18}O$ values of core MD07–3119 decrease only by ~0.2‰ during Event 1, reaching 4.3‰. A similar behavior can be observed in the $\delta^{13}C$ records obtained for the four cores; that is, a similarity between the shallower ones, compared to MD07–3119 (Figure 2a). The shallower cores show a sharp, near synchronous, $\delta^{13}C$ increase, indicating similar bottom water conditions, while the $\delta^{13}C$ increase recorded at

2,500 m, during Event 1, is small, leading to a significant ~0.6‰ difference between ~1,500 and 2,500 m (Figure 2a). From the end of the ACR to Event 2, the Cibicides $\delta^{13}C$ of the four cores increases up to 0.2‰ and 0.3‰, for MD07–3100 and MD07–3082, respectively, and to ~0‰ for core MD07–3088 and MD07–3119. These values are close within errors, but unlike during Event 1, there is no significant difference between the records from ~1,500 and 2,500 m.

Despite the uncertainties (30 μmol/kg) and the noise of the records, the reconstructed $[O_2]$ indicates the occurrence of a bottom water oxygen increase at the site of core MD07–3100 during Event 2 and the latest part of Event 1 (Figure 2c). A similar trend can be observed at the site of core MD07–3088, but the variation is hardly out of the uncertainties during Event 2 (Figure 2c).

During the deglaciation, the benthic foraminifera assemblage of core MD07–3100 is characterized by the decrease of *Uvigerina* spp, replaced by *T. angulosa* (Figure 3). It has been proposed that *T. angulosa* is an indicator of higher bottom water hydrodynamism, with coarser sediment grains (Harloff, & Mackensen, a., 1997; Mackensen et al., 1985; Mackensen et al., 1993; Schönfeld, 2002). On the other hand, the *Uvigerina* spp deglacial decrease does not indicate a limitation in the food supply as suggested by the relatively high benthic foraminifera Accumulation rates during this time interval (Figure S7). We also note the constant presence of epibenthic species such as *Cibicidoides* spp and the very low percentages of deep endobenthic taxa such as *Globobulimina* spp and *Chilostomella ovoidea* (Reuss, 1850). This indicates that the oxygen levels in the bottom water never drop to reach critical levels (i.e., anoxic) during the deglaciation (e.g., Fontanier et al., 2002; Jorissen et al., 1995), confirming the $[O_2]$ record of MD07–3100 (Figure 2c). Thus, these observations suggest that (i) the $[O_2]$ is not a limiting factor on the benthic foraminifera assemblages of MD07–3100 and (ii) during the deglaciation, *T. angulosa* occurrence at the site of core MD07–3100 could be related to enhanced bottom water hydrodynamism as this species has been associated to higher bottom current velocities and coarser grain size (Harloff, & Mackensen, a., 1997; Mackensen et al., 1985; Mackensen et al., 1993; Schönfeld, 2002).

Furthermore, the diversity index H (Shannon-Wiener index, Shannon, 1948) calculated from the benthic assemblages from core MD07–3100 (Figure S8) suggests that the deglacial bottom current velocity variations exert stressing condition on the benthic foraminifera assemblage, probably because of the enhanced bottom water hydrodynamic variations, promoting the increase of *T. angulosa* taxa. At the same time, this process could also have exported the organic matter laterally, generating unstable bottom water conditions that would reduce the microfaunal diversity (e.g., Martins et al., 2015).

Further south, the benthic foraminifera faunal record from core MD07–3082 (Figure 3) is different from MD07–3100 one, with *Cibicidoides* spp dominating the assemblage during the deglaciation, also probably indicating a complete change of the bottom water ventilation conditions and/or a variation in food supply at this site. These findings could suggest much more oxygenated bottom waters at the location of core MD07–3082 compared to MD07–3100.

At 2,500 m we do not observe a significant $[O_2]$ increase during upwelling Events 1 and 2, but only a slight increasing deglacial $[O_2]$ trend after ~14.3 kyr.

The $[O_2]$ increase (Figure 2c) at 1,500–1,700 m suggests that during Events 1 and 2 at the Antarctic divergence, more ventilated waters bathed these core depths in the SEP, compared to the Holocene and the late glacial.

Between 41°S and 36°S in the SEP, Muratli et al. (2010) indicated a decreasing ventilation of AAIW during the deglaciation. A sharp increase in authigenic Re concentrations is first observed in the shallower core record (ODP 1235, 500 m) at the beginning of Event 1, indicating probably a deepening of the AAIW core. A progressive increase of Re for the deeper core (ODP 1234) and decrease of authigenic Mn concentration for ODP 1233, in the modern core of AAIW (840 m depth) (Muratli et al., 2010, were probably associated with a southward displacement of the AAIW source region. The above scenario of larger O_2 and $\delta^{13}C$ increase at ~1,500/1,700 m compared to 2,500 m suggests a southward shift of AAIW convection area and a deepening of the AAIW, with the shallower cores being more influenced by the AAIW during Events 1 and 2. The $\delta^{13}C$ and $[O_2]$ records (Figures 2a and 2c) indicate that upwelling Event 2 after the ACR is slightly different than the one before, with core MD07–3082 already, or beginning to be, bathed by a more ventilated water mass, while MD07–3100 and MD07–3088 cores stay within the AAIW.

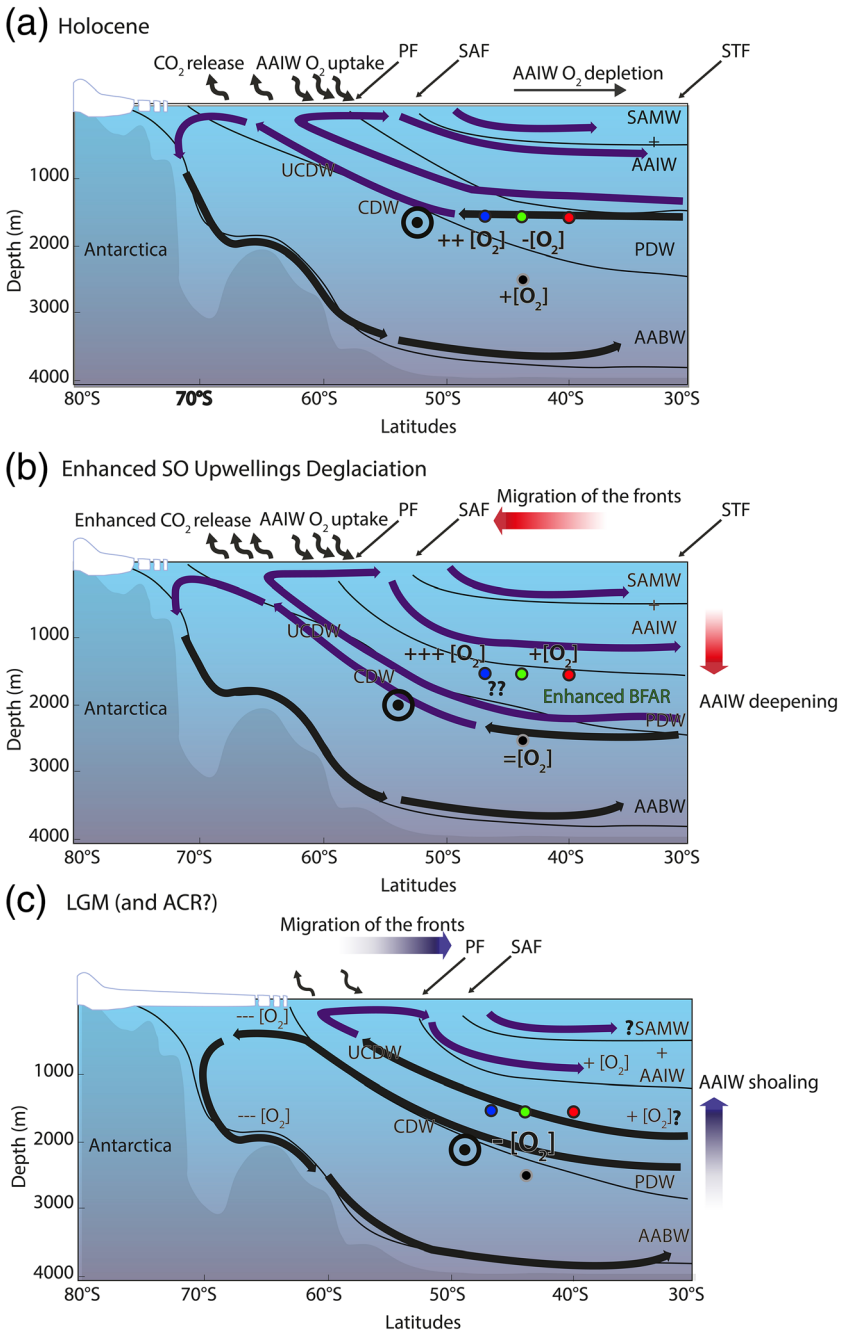

Figure 4. Suggested water masses ventilations and limit positions, on a latitudinal transect in the SEP. Antarctic bottom water, AABW; Antarctic intermediate water, AAIW; benthic foraminifera accumulation rates, BFAR; Pacific deep waters, PDW; polar front, PF; Subantarctic front, SAF; Subantarctic mode water, SAMW; subtropical front, STF; (upper) circumpolar deep water, (U)CDW. The black circled dot of the CDW indicates that this current flows out of the figure. The relative increase and decrease of the oxygen concentration near the considered cores, inferred from our reconstructions, are indicated by "+[O_2]" and "−[O_2]," respectively. The relative ventilation variations in the bottom panel are inferred from Muratli et al. (2010) and Martínez-Méndez et al. (2013) north of our study area and from Lu et al. (2016) near Antarctica.

5.3. ACR

From ~14.2 to 12.4 kyr, the $\delta^{13}C$ of the three shallow cores decreases, reaching similar values to core MD07–3119. Similarly, the O_2 concentration of core MD07–3088 and MD07–3100 also decreases during this period (Figures 2b and 2c). This small decrease in the oxygenation is accompanied by reduced current intensities as

suggested by the H index of core MD07–3100 (Figure S8). These observations point toward a return to a shallower position of the AAIW water mass and/or an overall $[O_2]$ decrease of the AAIW due to ventilation decrease and/or a northern shift of its formation area (Figure 4a; Haddam et al., 2018).

5.4. Holocene

The Holocene is characterized by a generally decreasing trend in the $\delta^{18}O$ values recorded in the four cores (Figure 2b). At the onset of the Holocene we observe a $\delta^{18}O$ gradient between these cores, in accordance with their depth location, indicating that this gradient is linked to the bottom water temperature and potentially higher salinity at 2,500 m depth that disappears progressively after ~4 kyr. The overall trend of the Holocene is also characterized by an increase of the $\delta^{13}C$ values (Figure 2a) of the four cores, reaching modern values, in accordance with the transition from AAIW to PDW (0.75‰ to 1.75‰; Bostock et al., 2010, and Figure S9). Yet markedly different $\delta^{13}C$ values between the northern cores and MD07–3082 can be observed (Figure 2b), indicating the influence of a more ventilated water mass at 49°S throughout the Holocene. The $[O_2]$ values of MD07–3100 indicate the influence of more oxygenated bottom water compared to the late glacial and the ACR, and slightly lower than during Events 1 and 2 of the deglaciation (Figure 2c). Aside from two high $[O_2]$ events at ~9 and ~4.6 kyrs recorded in core MD07–3119, the $[O_2]$ values related to the three shallower cores are similar, within the uncertainty limit and within modern values of ~135 μmol/kg at 41°S and 46°S, ~1,600 m depth, and of 150 μmol/kg at 2,500 m.

The bottom water ventilation at 49°S can be assessed qualitatively by the benthic foraminifera assemblages (e.g., Fontanier et al., 2002; Jorissen et al., 1995). The high percentages of *Cibicidoides* spp in core MD07–3082 (Figure 3b) indicate higher $[O_2]$/and-or lower food supply compared to the northern core MD07–3100 (and thus MD07–3088 as suggested by their similar $[O_2]$ records; Figure 2c) during the Holocene. Indeed, the benthic foraminifera content of MD07–3100 puts into evidence the constant dominance of *Uvigerina* spp and *Bulimina* spp, suggesting (i) high organic matter fluxes to the sea floor during the Holocene and/or (ii) less ventilated bottom waters compared to MD07–3082. From the comparison of the ventilation proxies of the four cores, we suggest that at the Early Holocene (~10 kyr), MD07–3082 was probably, under the influence of the UCDW, a more ventilated water mass than the upper limit of PDW that bathed the northern cores.

These observations suggest a schematic reconstruction of the geometry variation of the water masses at intermediate depth in the SEP (Figure 4). During the Late glacial (and probably the ACR), it appears, according to our records, that the three shallower cores were bathed by the lower part of the upper overturning cell, while MD07–3119 staying in the lower cell. This position leads us to place the limit between these cells between ~1,700 and ~2,500 m during the late glacial in the SEP (Figure 4). During upwelling Events 1 and 2 of the deglaciation, our findings suggest a deepening of the AAIW water mass. It seems that the upper overturning cell is destabilized before the lower overturning cell as suggested by our records at 2,500 m, probably induced by Southern Hemisphere warming strengthened by southern sea ice melting and southward jet migration feedbacks (Chiang et al., 2014; Chiang et al., 2018; Haddam et al., 2018). After the deglaciation, the shallower cores are progressively bathed by the lower cell's water masses. The two northernmost cores, MD07–3100 and MD07–3088, and the deep core MD07–3119 seem to be more influenced by the PDW, while southernmost core MD07–3082 is bathed by the CDW (Figure 4).

6. Conclusive Remarks

The location of our cores, at the boundary between AAIW, CDW, and PDW, allowed us to reconstruct both ventilation and depth expansion of these water masses. We suggest that over the past 22 kyr, the depth limit between the AAIW and CDW-PDW changed due to the ventilation fluctuations of the intermediate and deep water masses. The comparisons with local and sublocal oxygen reconstructions corroborate this view and indicate that there are three states of ventilation—AAIW/CDW-PDW depth limit between the late glacial, the deglaciation, and the Holocene, following the variations of the SO overturning changes.

During the Late glacial and the ACR, the AAIW/CDW-PDW boundary depth shoals, in the SEP, as its formation zone (the PF zone) moves slightly northward enhancing the influence of a $[O_2]$-depleted bottom water at our cores locations. During the deglaciation, the upper overturning cell is probably destabilized

before the lower overturning cell. During this period, the $\delta^{13}C$ increase, the $[O_2]$ enrichment of the AAIW, and the dominance of *T. angulosa* over the benthic assemblages (41°S, 1,500 m) indicate that Antarctic divergence upwelling Events 1 and 2 lead to a southward shift of AAIW and a deepening of the AAIW/CDW-PDW boundary along with a more vigorous AAIW ventilation as indicated by the modeling study of Chiang et al. (2018).

After Event 2 of the deglaciation, at the beginning of the Holocene, core MD07–3082 was influenced by more ventilated CDW, while MD07–3088 and MD07–3100 show PDW characteristics, indicating that the AAIW/PDW limit shoaled and PDW oxygen increased from ~14.3 kyrs to the middle Holocene. The comparison with the regional $[O_2]$ reconstruction studies, at different depths, and different distances from AAIW source region enables the reconstruction of the latitudinal and depth changes in the AAIW over the deglaciation, highlighting the control of the SO overturning variations on the AAIW production rates and the depth limit since the LGM.

Data Availability Statement

The data presented in this article will be available on the Pangaea repository (https://doi.pangaea.de/10.1594/PANGAEA.917846).

Acknowledgments

We thank the captains and the crew of the R/V Marion Dufresne during the PACHIDERME cruise for their help retrieving the MD-3082, MD-3088, MD-3100, and MD-3119 cores. This manuscript has been improved by the comments of Helen C. Bostock, an anonymous reviewer, and William R. Gray. Financial support was made by the French ministry of research and higher education and the French-Swedish project on SO VR-349-2012-6278, and ECOSUD, SEPORA INSU Project.

References

Anderson, R. F., Ali, S., Bradtmiller, L. I., Nielsen, S. H. H., Fleisher, M. Q., Anderson, B. E., & Burckle, L. H. (2009). Wind-driven upwelling in the Southern Ocean and the deglacial rise in atmospheric CO2. *Science (New York, N.Y.)*, *323*(5920), 1443–1448. https://doi.org/10.1126/science.1167441

Bostock, H. C., Barrows, T. T., Carter, L., Chase, Z., Cortese, G., Dunbar, G. B., et al. (2013). A review of the Australian-New Zealand sector of the Southern Ocean over the last 30 ka (Aus-INTIMATE project). *Quaternary Science Reviews*, *74*, 35–57. https://doi.org/10.1016/j.quascirev.2012.07.018

Bostock, H. C., Opdyke, B. N., & Williams, M. J. M. (2010). Characterising the intermediate depth waters of the Pacific Ocean using δ13C and other geochemical tracers. *Deep Sea Research Part I: Oceanographic Research Papers*, *57*(7), 847–859. https://doi.org/10.1016/j.dsr.2010.04.005

Bostock, H. C., Opdyke, B. N., Gagan, M. K., & Fifield, L. K. (2004). Carbon isotope evidence for changes in Antarctic intermediate water circulation and ocean ventilation in the Southwest Pacific during the last deglaciation. *Paleoceanography*, *19*, PA4013. https://doi.org/10.1029/2004PA001047

Bostock, H. C., Sutton, P. J., Williams, M. J. M., & Opdyke, B. N. (2013). Reviewing the circulation and mixing of Antarctic intermediate water in the South Pacific using evidence from geochemical tracers and Argo float trajectories. *Deep Sea Research Part I: Oceanographic Research Papers*, *73*, 84–98. https://doi.org/10.1016/j.dsr.2012.11.007

Boyer, T. P., Antonov, J. I., Baranova, O. K., Coleman, C., Garcia, H. E., Grodsky, A., et al. (2013). *World Ocean Database 2013*, (208). Silver Spring, MD: NOAA Printing Officce, (NOAA Atlas NESDIS, 72). http://hdl.handle.net/11329/357

Boyle, E. A., & Keigwin, L. (1987). North Atlantic thermohaline circulation during the past 20,000 years linked to high-latitude surface temperature. *Nature*, *330*(6143), 35–40. https://doi.org/10.1038/330035a0

Bronk Ramsey, C., & Lee, S. (2013). Recent and planned developments of the program OxCal. *Radiocarbon*, *55*(3–4), 720–730. https://doi.org/10.2458/azu_js_rc.55.16215

Chiang, J. C. H., Lee, S. Y., Putnam, A. E., & Wang, X. (2014). South Pacific Split jet, ITCZ shifts, and atmospheric north-south linkages during abrupt climate changes of the last glacial period. *Earth and Planetary Science Letters*, *406*, 233–246. https://doi.org/10.1016/j.epsl.2014.09.012

Chiang, J. C. H., Tokos, K. S., Lee, S.-Y., & Matsumoto, K. (2018). Contrasting impacts of the South Pacific Split jet and the southern annular mode modulation on Southern Ocean circulation and biogeochemistry. *Paleoceanography and Paleoclimatology*, *33*(1), 2–20. https://doi.org/10.1002/2017PA003229

Croudace, I. W., & Rothwell, R. G. (2015). In I. W. Croudace, & R. G. Rothwell (Eds.), *Micro-XRF studies of sediment cores*, (Vol. 17). Netherlands: Springer. https://doi.org/10.1007/978-94-017-9849-5

Curry, W. B., Duplessy, J. C., Labeyrie, L. D., & Shackleton, N. J. (1988). Changes in the distribution of δ 13C of deep water ΣCO2 between the last glaciation and the Holocene. *Paleoceanography*, *3*(3), 317–341. https://doi.org/10.1029/PA003i003p00317

Curry, W. B., & Oppo, D. W. (2005). Glacial water mass geometry and the distribution of δ 13C of ΣCO2 in the western Atlantic Ocean. *Paleoceanography*, *20*, PA1017. https://doi.org/10.1029/2004PA001021

Cushman, J. A. (1927). An outline of reclassification of the foraminifera. *Contributions from the Cushman Laboratory for Foraminiferal Research*, *3*(1), 1–105.

d'Orbigny, A. D. (1826). Tableau méthodique de la classe des Céphalopodes. *Annales des Sciences Naturelles*, *7*(96–169), 245–314. Retrieved from. http://biodiversitylibrary.org/page/5753959

d'Orbigny, A. D. (1839). Foraminifères, in de la Sagra R., Histoire physique, politique et naturelle de l'ile de Cuba. A. Bertrand., 1–224. Retrieved from https://books.google.pt/books?id=KpVeAAAAcAAJ&pg

d'Orbigny, A. D. (1846). *Foraminifères fossiles du bassin tertiaire de Vienne.*, 312. Retrieved from. https://archive.org/details/bub_gb_JKpAAAAAcAAJ

Duchamp-Alphonse, S., Siani, G., Michel, E., Beaufort, L., Gally, Y., & Jaccard, S. L. (2018). Enhanced Ocean-atmosphere carbon partitioning via the carbonate counter pump during the last deglacial. *Nature Communications*, *9*(1), 2396. https://doi.org/10.1038/s41467-018-04625-7

Duplessy, J., Labeyrie, L., & Waelbroeck, C. (2002). Constraints on the ocean oxygen isotopic enrichment between the Last Glacial Maximum and the Holocene: Paleoceanographic Implications. *Quaternary Science Reviews* (Vol. *21*, pp. 315–330).

Duplessy, J. C., Shackleton, N. J., Fairbanks, R. G., Labeyrie, L., Oppo, D., & Kallel, N. (1988). Deepwater source variations during the last climatic cycle and their impact on the global Deepwater circulation. *Paleoceanography*, *3*(3), 343–360. https://doi.org/10.1029/PA003i003p00343

Durand, A., Chase, Z., Noble, T. L., Bostock, H., Jaccard, S. L., Townsend, A. T., et al. (2018). Reduced oxygenation at intermediate depths of the Southwest Pacific during the Last Glacial Maximum. *Earth and Planetary Science Letters*, *491*, 48–57. https://doi.org/10.1016/j.epsl.2018.03.036

Elderfield, H., Greaves, M., Barker, S., Hall, I. R., Tripati, A., Ferretti, P., et al. (2010). A record of bottom water temperature and seawater δ18O for the Southern Ocean over the past 440kyr based on mg/Ca of benthic foraminiferal Uvigerina spp. *Quaternary Science Reviews*, *29*(1–2), 160–169. https://doi.org/10.1016/j.quascirev.2009.07.013

Elmore, A. C., McClymont, E. L., Elderfield, H., Kender, S., Cook, M. R., Leng, M. J., et al. (2015). Antarctic intermediate water properties since 400 ka recorded in infaunal (Uvigerina peregrina) and epifaunal (Planulina wuellerstorfi) benthic foraminifera. *Earth and Planetary Science Letters*, *428*, 193–203. https://doi.org/10.1016/j.epsl.2015.07.013

Ferrari, R., Jansen, M. F., Adkins, J. F., Burke, A., Stewart, A. L., & Thompson, A. F. (2014). Antarctic Sea ice control on ocean circulation in present and glacial climates. *Proceedings of the National Academy of Sciences of the United States of America*, *111*(24), 8753–8758. https://doi.org/10.1073/pnas.1323922111

Fischer, H., Schmitt, J., Lüthi, D., Stocker, T. F., Tschumi, T., Parekh, P., et al. (2010). The role of Southern Ocean processes in orbital and millennial CO2 variations—A synthesis. *Quaternary Science Reviews*, *29*(1–2), 193–205. https://doi.org/10.1016/j.quascirev.2009.06.007

Fontanier, C., Jorissen, F. J., Licari, L., Alexandre, A., Anschutz, P., & Carbonel, P. (2002). Live benthic foraminiferal faunas from the Bay of Biscay: Faunal density, composition, and microhabitats. *Deep-Sea Research Part I: Oceanographic Research Papers*, *49*(4), 751–785. https://doi.org/10.1016/S0967-0637(01)00078-4

Fornasini, C. (1902). Contributo a la conoscenza de le Bulimine adriatiche. *Reale Academia Delle Scienze Dell'Instituto Di Bologna, Memorie Delle Scienze Naturali*, *5*(9), 371–381.

Garreaud, R., Lopez, P., Minvielle, M., & Rojas, M. (2013). Large-scale control on the Patagonian climate. *Journal of Climate*, *26*(1), 215–230. https://doi.org/10.1175/JCLI-D-12-00001.1

Guérin-Méneville, F. E. (1832). Iconographie du Règne Animal de G. Cuvier, ou représentation d'après nature de l'une des espèces les plus remarquables, et souvent non encore figurées, de chaque genre d'animaux, avec un texte descriptif mis au courant de la science. In *Ouvrage pouvant servi*, (pp. 1–48). Paris and London: J.B. Baillière.

Haddam, N. A., Siani, G., Michel, E., Kaiser, J., Lamy, F., Duchamp-Alphonse, S., et al. (2018). Changes in latitudinal sea surface temperature gradients along the southern Chilean margin since the last glacial. *Quaternary Science Reviews*, *194*, 62–76. https://doi.org/10.1016/j.quascirev.2018.06.023

Harloff, J., & Mackensen, a. (1997). Recent benthic foraminiferal associations and ecology of the Scotia Sea and argentine basin. *Marine Micropaleontology*, *31*(1–2), 1–29. https://doi.org/10.1016/S0377-8398(96)00059-X

Hartin, C. A., Fine, R. A., Sloyan, B. M., Talley, L. D., Chereskin, T. K., & Happell, J. (2011). Formation rates of Subantarctic mode water and Antarctic intermediate water within the South Pacific. *Deep-Sea Research Part I*, *58*(5), 524–534. https://doi.org/10.1016/j.dsr.2011.02.010

Hasson, A., Koch-Larrouy, A., Morrow, R., Juza, M., & Penduff, T. (2012). The origin and fate of mode water in the southern Pacific Ocean. *Ocean Dynamics*, *62*(3), 335–354. https://doi.org/10.1007/s10236-011-0507-3

Hermelin, J. O. R., & Shimmield, G. B. (1990). The importance of the oxygen minimum zone and sediment geochemistry in the distribution of recent benthic foraminifera in the Northwest Indian Ocean. *Marine Geology*, *91*(1-2), 1–29. https://doi.org/10.1016/0025-3227(90)90130-C

Herraiz-Borreguero, L., & Rintoul, S. R. (2011). Subantarctic mode water: Distribution and circulation. *Ocean Dynamics*, *61*(1), 103–126. https://doi.org/10.1007/s10236-010-0352-9

Hines, S. K. V., Southon, J. R., & Adkins, J. F. (2015). A high-resolution record of Southern Ocean intermediate water radiocarbon over the past 30,000 years. *Earth and Planetary Science Letters*, *432*, 46–58. https://doi.org/10.1016/j.epsl.2015.09.038

Hodell, D. a., Venz, K. a., Charles, C. D., & Ninnemann, U. S. (2003). Pleistocene vertical carbon isotope and carbonate gradients in the South Atlantic sector of the Southern Ocean. *Geochemistry, Geophysics, Geosystems*, *4*(1), 1004. https://doi.org/10.1029/2002GC000367

Hogg, A. G., Hua, Q., Blackwell, P. G., Niu, M., Buck, C. E., Guilderson, T. P., et al. (2013). SHCal13 Southern Hemisphere calibration, 0–50 000 years cal BP. *Radiocarbon*, *55*, 1–15.

Hoogakker, B. A., Elderfield, H., Schmiedl, G., McCave, I. N., & Rickaby, R. E. M. (2015). Glacial–interglacial changes in bottom-water oxygen content on the Portuguese margin. *Nature Geoscience*, *8*(January), 40–43. https://doi.org/10.1038/ngeo2317

Jaccard, S. L., & Galbraith, E. D. (2011). Large climate-driven changes of oceanic oxygen concentrations during the last deglaciation. *Nature Geoscience*, *5*(2), 151–156. https://doi.org/10.1038/NGEO1352

Jannink, N., Zachariasse, W. J., & Van der Zwaan, G. J. (1998). Living (rose Bengal stained) benthic foraminifera from the Pakistan continental margin (northern Arabian Sea). *Deep-Sea Research Part I*, *45*(9), 1483–1513. https://doi.org/10.1016/S0967-0637(98)00027-2

Jorissen, F. J., De Stigter, H. C., & Widmark, J. G. V. (1995). A conceptual model explaining benthic foraminiferal microhabitats. *Marine Micropaleontology*, *26*(1–4), 3–15. https://doi.org/10.1016/0377-8398(95)00047-X

Kalnay, E., Kanamitsu, M., Kistler, R., Collins, W., Deaven, D., Gandin, L., et al. (1996). The NCEP/NCAR 40-year reanalysis project. *Bulletin of the American Meteorological Society*, *77*, 471–431.

Keeling, R. F., & Stephens, B. B. (2001). Antarctic Sea ice and the control of Pleistocene climate instability. *Paleoceanography*, *16*(1), 112–131. https://doi.org/10.1029/2000PA000529

Kissel, C. (2007). MD 159-PACHIDERME IMAGES XV, Cruise Report 06.02.07-28.02.07. *Plouzané: Institut Polaire Français Paul Émile Victor*, 1, 84.

Labeyrie, L., Waelbroeck, C., Cortijo, E., Michel, E., & Duplessy, J.-C. (2005). Changes in deep water hydrology during the last Deglaciation. *Comptes Rendus Geoscience*, *337*(10–11), 919–927. https://doi.org/10.1016/j.crte.2005.05.010

Le Calvez, Y. (1958). Rev. Trav. Inst. Pêches Maritimes. Revue des travaux de l'Institut des pêches maritimes (Vol. 22).

Leth, O., Shaffer, G., & Ulloa, O. (2004). Hydrography of the eastern South Pacific Ocean: Results from the Sonne 102 cruise, May–June 1995. *Deep Sea Research Part II: Topical Studies in Oceanography*, *51*(20–21), 2349–2369. https://doi.org/10.1016/j.dsr2.2004.08.009

Loeblich, A. R. J., & Tappan, H. (1987). *Foraminiferal genera and their classification* (Vol. 869). New York: Van Norstrand Reinhold Company.

Lu, Z., Hoogakker, B. A. A., Hillenbrand, C.-D., Zhou, X., Thomas, E., Gutchess, K. M., et al. (2016). Oxygen depletion recorded in upper waters of the glacial Southern Ocean. *Nature Communications*, *7*(1), 11,146. https://doi.org/10.1038/ncomms11146

Mackensen, A., Sejrup, H. P., & Jansen, E. (1985). The distribution of living benthic foraminifera on the continental slope and rise off Southwest Norway. *Marine Micropaleontology*, *9*(4), 275–306. https://doi.org/10.1016/0377-8398(85)90001-5

Mackensen, Andreas, Hubberten, H., Bickert, T., & Ftitterer, D. K. (1993). The δ13C in benthic foraminiferal tests of Fontbotia wuellerstorfi (Schwager) relative to the δ13C of dissolved inorganic carbon in the Southern Ocean deep water : Implications for glacial ocean circulation models. *Paleocanography*, *8*, 587–610.

Martínez-Méndez, G., Hebbeln, D., Mohtadi, M., Lamy, F., De Pol-Holz, R., Reyes-Macaya, D., & Freudenthal, T. (2013). Changes in the advection of Antarctic intermediate water to the northern Chilean coast during the last 970 kyr. *Paleoceanography*, *28*, 607–618. https://doi.org/10.1002/palo.20047

Martins, M. V. A., Quintino, V., Tentúgal, R. M., Frontalini, F., Miranda, P., Laut, L. L. M.et al.. (2015). Characterization of bottom hydrodynamic conditions on the central western Portuguese continental shelf based on benthic foraminifera and sedimentary parameters. *Marine Environmental Research*, *109*, 52–68. https://doi.org/10.1016/j.marenvres.2015.06.006

McCartney, M. S. (1977). Subantarctic mode water. *Deep-Sea Research*, *24*, 103–119.

McCartney, M. S. (1982). The subtropical recirculation of mode waters. *Journal of Marine Research*, *40*(S-23), 427–464.

Michel, E., Labeyrie, L., Duplessy, J. C., Gorfti, N., Labracherie, M., & Turon, J. L. (1995). Could deep subantarctic convection feed the world deep basins during the Last Glacial Maximum? *Paleoceanography*, *10*(5), 927–941. https://doi.org/10.1029/95PA00978

Muratli, J. M., Chase, Z., Mix, A. C., & McManus, J. (2010). Increased glacial-age ventilation of the Chilean margin by Antarctic intermediate water. *Nature Geoscience*, *3*(1), 23–26. https://doi.org/10.1038/ngeo715

NASA Goddard Space Flight Center Ocean biology processing group (OBPG) (2014). *Sea-viewing Wide Field-of-view Sensor (SeaWiFS) ocean color data*. Greenbelt, MD, USA: Maintained by NASA Ocean Biology Distibuted Active Archive Center (OB.DAAC), Goddard Space Flight Center, Greenbelt MDNASA OB.DAAC. 10.5067/ORBVIEW-2/SEAWIFS_OC.2014.0

Orsi, A. H., Whitworth, T., & Nowlin, W. D. (1995). On the meridional extent and fronts of the Antarctic circumpolar current. *Deep Sea Research Part I: Oceanographic Research Papers*, *42*(5), 641–673. https://doi.org/10.1016/0967-0637(95)00021-W

Pahnke, K., & Zahn, R. (2005). Southern hemisphere water mass conversion linked with North Atlantic climate variability. *Science*, *307*(5716), 1741–1746. https://doi.org/10.1126/science.1102163

Park, Y. -H., Park, T., Kim, T. -W., Lee, S. -H., Hong, C. -S., Lee, J. -H., et al. (2019). Observations of the Antarctic circumpolar current over the Udintsev fracture zone, the narrowest choke point in the Southern Ocean. *Journal of Geophysical Research: Oceans*, 2019JC015024, *124*, 4511–4528. https://doi.org/10.1029/2019JC015024

Parker, F. L. (1953). Distribution of the foraminifera in the Northwest Gulf of Mexico. *Bulletin of the Museum of Comparative Zoology*, *111*, 453–588.

Peterson, R. G., & Stramma, L. (1991). Upper-level circulation in the South-Atlantic Ocean. *Progress in Oceanography*, *26*(1), 1–73. https://doi.org/10.1016/0079-6611(91)90006-8

Pinochet, A., Garcés-Vargas, J., Lara, C., & Olguín, F. (2019). Seasonal variability of upwelling off central-southern Chile. *Remote Sensing*, *11*(15), 1737. https://doi.org/10.3390/rs11151737

Qu, T., Gao, S., Fukumori, I., Fine, R. A., & Lindstrom, E. J. (2008). Subduction of South Pacific waters. *Geophysical Research Letters*, *35*, L02610. https://doi.org/10.1029/2007GL032605

Reuss, A. E. (1850). Neues Foraminiferen aus den Schich-ten des österreichischen Tertiärbeckens. In *DenkSchriften Der Kaiserlichen Akademie Del Wissenschaften, Mathematisch-Naturwissenschafliche Classe* (Vol. 1, pp. 365–390). Wien, Austria.

Reuss, A. E. (1851). Ueber die fossilen Foraminiferen und Entomostraceen der Septarienthone der Umgegend von Berlin. In *Zeitschrift Der Deutschen Geologischen Gesellschaft* (Vol. 3, 1, 49–92). Germany.

Ribbe, J., & Tomczak, M. (1997). On convection and the formation of Subantarctic mode water in the Fine resolution Antarctic model (FRAM). *Journal of Marine Systems*, *13*(1–4), 137–154. https://doi.org/10.1016/S0924-7963(96)00119-4

Rintoul, S., Hughes, C., & Olbers, D. (2001). The Antarctic circumpolar current system BT—Ocean circulation and climate. *Ocean Circulation and Climate.*, *65*(4), 377–383. https://doi.org/10.1002/ajp.20122

Rintoul, S. R., & England, M. H. (2002). Ekman transport dominates local air-sea fluxes in driving variability of Subantarctic mode water. *Journal of Physical Oceanography*, *32*(5), 1308–1321. https://doi.org/10.1175/1520-0485(2002)032%3C1308:ETDLAS%3E2.0.CO;2

Ronge, T. A., Steph, S., Tiedemann, R., Prange, M., Merkel, U., Nürnberg, D., & Kuhn, G. (2015). Pushing the boundaries: Glacial/interglacial variability of intermediate and deep waters in the Southwest Pacific over the last 350,000 years. *Paleoceanography*, *30*, 23–38. https://doi.org/10.1002/2014PA002727

Rzehak, A. (1886). Die Foraminiferen fauna der Neogenformation der Umgebung von Mähr.-Ostrau. In *Verhandlungen des naturforschenden Vereines in Brünn* (Vol. 24, pp. 77–126). Czechoslovakia: Naturforschender Verein in Brünn. https://www.biodiversitylibrary.org/page/47820383#page/118/mode/1up

Sallée, J.-B., Speer, K., Rintoul, S., & Wijffels, S. (2010). Southern Ocean thermocline ventilation. *Journal of Physical Oceanography*, *40*(3), 509–529. https://doi.org/10.1175/2009JPO4291.1

Schlitzer, R. (2020). *Ocean Data View*, odv.awi.de

Schönfeld, J. (2002). Recent benthic foraminiferal assemblages in deep high-energy environments from the Gulf of Cadiz (Spain). *Marine Micropaleontology*, *44*(3–4), 141–162. https://doi.org/10.1016/S0377-8398(01)00039-1

Schwager, C. (1866). Fossile Foraminifera von Kar Nikobar, Reise der Österreichischen Fregatte Novara um die Erde in den Jahren 1857, 1858, 1859 unter den Befehlen des Commodore B. Von Wüllerstorf-Urbair. *Geologischer Theil. Geologische Beobachtungen. Paläontologtsche Miltheilungen*, *2*(I), 187–268.

Shannon, C. E. (1948). A mathematical theory of communication. *Bell System Technical Journal*, *27*(4), 623–656. https://doi.org/10.1002/j.1538-7305.1948.tb00917.x

Siani, G., Michel, E., De Pol-Holz, R., Devries, T., Lamy, F., et al. (2013). Carbon isotope records reveal precise timing of enhanced Southern Ocean upwelling during the last deglaciation. *Nature Communications*, *4*(1), 2758. https://doi.org/10.1038/ncomms3758

Silva, N., Rojas, N., & Fedele, A. (2009). Water masses in the Humboldt current system: Properties, distribution, and the nitrate deficit as a chemical water mass tracer for equatorial subsurface water off Chile. *Deep-Sea Research II*, *56*(16), 1004–1020. https://doi.org/10.1016/j.dsr2.2008.12.013

Sloyan, B. M., & Rintoul, S. R. (2001). Circulation, renewal, and modification of Antarctic mode and intermediate water*. *Journal of Physical Oceanography*, *31*(4), 1005–1030. https://doi.org/10.1175/1520-0485(2001)031%3C1005:CRAMOA%3E2.0.CO;2

Sloyan, B. M., Talley, L. D., Chereskin, T. K., Fine, R., & Holte, J. (2010). Antarctic intermediate water and Subantarctic mode water formation in the Southeast Pacific: The role of turbulent mixing. *Journal of Physical Oceanography*, *40*(7), 1558–1574. https://doi.org/10.1175/2010JPO4114.1

Stramma, L., Peterson, R. G., & Tomczak, M. (1995). The South Pacific current. *Journal of Physical Oceanography*, *25*(1), 77–91. https://doi.org/10.1175/1520-0485(1995)025%3C0077:TSPC%3E2.0.CO;2

Talley, L. (2013). Closure of the global overturning circulation through the Indian, Pacific, and southern oceans: Schematics and transports. *Oceanography*, *26*(1), 80–97. https://doi.org/10.5670/oceanog.2013.07

Talley, L. D. (1999. In Some aspects of ocean heat transport by the shallow, intermediate and deep overturning circulations. In P. U. Clark, R. S. Webb, & L. D. Keigwin (Eds.), *Mechanisms of global climate change at millenial time scales*, *Geophysical Monograph Series* (Vol. 112, 1–22).American Geophysical Union.

Talley, L. D. (2008). Freshwater transport estimates and the global overturning circulation: Shallow, deep and throughflow components. *Progress in Oceanography*, *78*(4), 257–303. https://doi.org/10.1016/j.pocean.2008.05.001

Tapia, R., Nürnberg, D., Ronge, T., & Tiedemann, R. (2015). Disparities in glacial advection of Southern Ocean intermediate water to the South Pacific gyre. *Earth and Planetary Science Letters*, *410*, 152–164. https://doi.org/10.1016/j.epsl.2014.11.031

Toggweiler, J. R., Russell, J. L., & Carson, S. R. (2006). Midlatitude westerlies, atmospheric CO2, and climate change during the ice ages. *Paleoceanography*, *21*, PA2005. https://doi.org/10.1029/2005PA001154

Toggweiler, J. R. (1999). Variation of atmospheric CO2 by ventilation of the ocean's deepest water. *Paleoceanography*, *14*(5), 571–588. https://doi.org/10.1029/1999PA900033

Tomczak, M., & Godfrey, J. S. (1994). Antarctic oceanography. In *Regional Oceanography* (pp. 67–87). Elsevier. https://doi.org/10.1016/B978-0-08-041021-0.50010-2

Tomczak, M., & Godfrey, J. T. (2001). Adjacent seas of the Indian Ocean and the Australasian Mediterranean Sea (the Indonesian throughflow). *Regional Oceanography*, (December), 220–228. https://doi.org/10.1016/B978-0-08-041021-0.50017-5

Trauth, F. (1918). In *Das Eozanvorkommen bei Radstadt im Pongou und seine Beziehungen zu den gleichalterigen Ablagerungen bei Kirchberg am Wechsel und Wimpassing am Leithagebirge* (Vol 95, 171–278). Wien, Austria: Kaiserliche Akademie der Wissenschaften, Mathematisch-Naturwissenschaftliche Classe, Denkschriften.

Tsuchiya, M., & Talley, L. D. (1998). A Pacific hydrographic section at 88°W: Water-property distribution. *Journal of Geophysical Research*, *103*(C6), 12,899–12,918. https://doi.org/10.1029/97JC03415

Waelbroeck, C., Labeyrie, L., Michel, E., Duplessy, J. C., McManus, J. F., Lambeck, K., et al. (2002). Sea-level and deep water temperature changes derived from benthic foraminifera isotopic records. *Quaternary Science Reviews*, *5*(2), 318–319. https://doi.org/10.1016/j.hrthm.2007.04.016

Williamson, W. C. (1858). *On the recent foraminifera of Great Britain* (Vol. 107). London: Ray Society.